


 Cite this: *RSC Adv.*, 2023, **13**, 11311

Magneto-structural studies on a number of doubly end-on cyanate and azide bridged dinuclear nickel(II) complexes with $\{N_3O\}$ donor Schiff base ligands[†]

 Narayan Ch. Jana, ^a Marko Jagodič, ^b Paula Brandão, ^c Moumita Patra, ^a Radovan Herchel, ^d Zvonko Jagličić ^{be} and Anangamohan Panja ^{*af}

Two new doubly $\mu_{1,1}$ -N₃ bridged (**1** and **3**) and six new doubly $\mu_{1,1}$ -NCO bridged Ni^{II} complexes (**2**, **4**–**8**) with six different N₃O donor Schiff base ligands have been synthesized and magneto-structurally characterized. All these neutral complex molecules are isostructural and constitute edge sharing bioctahedral structures. Magnetic studies revealed that all these complexes exhibit ferromagnetic interaction through bridging pseudohalides with ferromagnetic coupling constant *J* being significantly higher for azide-bridged complexes than that of the cyanate analogues. This is consistent with the literature reported data and also the presence of polarizable π systems and two different N and O donor atoms in cyanate ion, rendering it a poor magnetic coupler in comparison to azide analogues. Although, the magneto-structurally characterized doubly $\mu_{1,1}$ -N₃ bridged Ni^{II} complexes are abundant, only few such complexes with $\mu_{1,1}$ -bridging NCO[–] ions are reported in the literature. Remarkably, addition of these six new examples in this ever-growing series of doubly $\mu_{1,1}$ -NCO bridged systems gives us an opportunity to analyse the precise magneto-structural correlation in this system, showing a general trend in which the *J* value increases with an increase in bridging angles. Therefore, the high degree of structural and magnetic resemblances by inclusion of six new examples in this series is the major achievement of the present work. An elaborate DFT study was performed resulting in magneto-structural correlation showing that nature and value of the *J*-parameter is defined not only by Ni–N_b–Ni bond angles, but an important role is also played by the Ni1–Ni2–N_b–X_t dihedral angle (N_b and X_t are bridging N and terminal N or O atom of bridging ligands, respectively).

 Received 3rd February 2023
 Accepted 24th March 2023

 DOI: 10.1039/d3ra00737e
rsc.li/rsc-advances

Introduction

Di- and poly-nuclear transition metal complexes with organic ligands have been widely studied because of their applications in various fields including bioinorganic chemistry and

magnetic materials.^{1–7} In such metal complexes, the paramagnetic centres are either bridged by endogenous bridges such as phenolate ion or exogenous bridging ligands *viz.* hydroxide, alkoxide, carboxylate and pseudohalide groups or by a combination of both.^{8–10} Among the different bridging ligands, pseudohalides particularly azide ions, are the most investigated ones due to their versatile coordination abilities that lead to huge structural diversities and remarkable magnetic properties.¹¹ In this regard, pseudohalide-bridged Ni^{II} complexes have attracted considerable attention in the field of molecular magnetism because of the presence of significant magnetic anisotropy in Ni^{II} ions, associated with the second order spin-orbit coupling, and because of the occurrence of possible high spin ground states through ferromagnetic interactions among Ni^{II} ions, mediated by the bridging pseudohalides, which are the essential criteria for displaying single-molecule magnetic behaviour.^{12–16} It is well known that the end-to-end (EE, $\mu_{1,3}$) bridging mode usually propagates anti-ferromagnetic (AF) interaction, while the end-on (EO, $\mu_{1,1}$) bridging azide ion transmits ferromagnetic (F) coupling

^aDepartment of Chemistry, Panskura Banamali College, Panskura RS, WB 721152, India. E-mail: ampanja@yahoo.co.in

^bInstitute of Mathematics, Physics and Mechanics, Jadranska 19, 1000 Ljubljana, Slovenia

^cDepartment of Chemistry, CICECO-Aveiro Institute of Materials, University of Aveiro, 3810-193 Aveiro, Portugal

^dDepartment of Inorganic Chemistry, Faculty of Science, Palacký University, 17. Listopadu 12, 77146 Olomouc, Czech Republic

^eFaculty of Civil and Geodetic Engineering, University of Ljubljana, Jamova 2, 1000 Ljubljana, Slovenia

^fDepartment of Chemistry, Gokhale Memorial Girls' College, 1/1 Harish Mukherjee Road, Kolkata-700020, India

[†] Electronic supplementary information (ESI) available: Fig. S1–S12, Table S1† and XYZ coordinated of model complexes used for DFT calculations. CCDC 2238074–2238081 for complexes **1**–**8**. For ESI and crystallographic data in CIF or other electronic format see DOI: <https://doi.org/10.1039/d3ra00737e>.



between Ni^{II} ions, indicating that the introduction of more and more EO bridging azide ions is prerequisite for developing better molecule-based magnetic materials.¹¹ Unlike azide ion, other heteroatomic pseudohalides, particularly cyanate ion, with polarizable π systems and two different N and O donor atoms, which can coordinate the metal ions through either of the heteroatoms, or both, are less versatile than the azide ion.^{17–23} Therefore, in contrast to the vast chemistry of azide-bridged complexes, magneto-structurally characterised compounds with cyanate ion are very limited.^{17–23} Consequently, unlike azide-bridged analogues, a sophisticated magneto-structural correlation is yet to be established for cyanate-bridged Ni^{II} systems, and therefore, it requires further attention.^{24,25} However, going through the only few examples available in the literature, one can assess that cyanate ion with EO bridging mode usually propagates ferromagnetic interaction between Ni^{II} centres in a similar way that azide ion does, but weakly, while a mixed immersion has been observed through EE bridging mode.^{17–23}

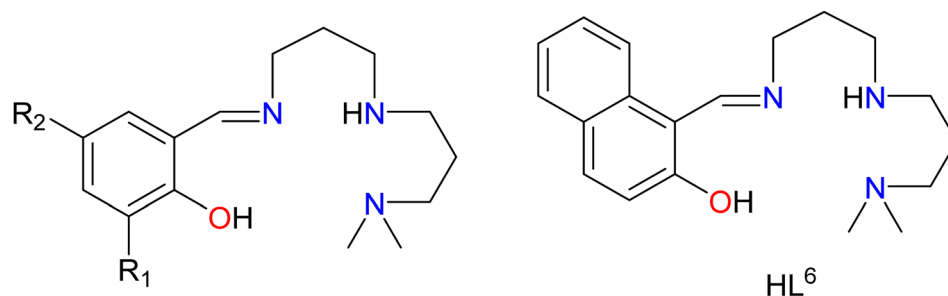
Although it is clear that the EO bridging mode of pseudohalides is crucial for developing better molecule-based magnetic materials with high spin ground state, it is difficult to control the bridging motif of the pseudohalides in the resulting complexes as it is influenced by several factors including nature of the organic ligands. Among several organic ligands, Schiff-base ligands have been extensively utilised for the development of a large numbers of Ni^{II} clusters with interesting structures and magnetic properties because of their synthetic simplicity and tuneable stereo-electronic properties by incorporating different amine and carbonyl counterparts.²⁶ Our recent studies disclosed that Schiff base ligands with N_3O donor sets derived from condensation of salicylaldehyde or its derivative with *N,N*-dimethylpropylenetriamine are capable to produce doubly EO azide or cyanate bridged ferromagnetically coupled dinuclear Ni^{II} complexes.^{20,22,23} Therefore, we anticipated that a large numbers of EO cyanate-bridged Ni^{II} complexes can be synthesised using different carbonyl

components of the Schiff base ligands derived from this triamine, which not only add few more examples to the only limited members of such complexes reported in the literature, but it is a possibility to establish precise magneto-structural correlation in this system. Consequently, in this present endeavour, a series of tetradentate N_3O donor Schiff base (HL^1 – HL^6 , Scheme 1), derived from the condensation reaction of *N,N*-dimethylpropylenetriamine with different carbonyl components, namely 2-hydroxy-3-methoxy-5-methylbenzaldehyde, 2-hydroxy-3-methoxybenzaldehyde, 5-nitrosalicylaldehyde, 5-bromo-3-methoxysalicylaldehyde, 4-(diethylamino)salicylaldehyde and 2-hydroxy-1-naphthaldehyde, have been utilised to prepare closely related EO cyanate-bridged Ni^{II} complexes. Furthermore, two EO azide-bridged Ni^{II} complexes with Schiff base HL^1 and HL^2 were produced to compare its magnetic transmitting ability with analogues EO cyanate-bridged Ni^{II} complexes. Herein, the structures and magnetic properties of eight new complexes $[\text{Ni}_2(\text{L}^1)_2(\mu_{1,1}\text{-N}_3\text{O})_2]$ (1), $[\text{Ni}_2(\text{L}^1)_2(\mu_{1,1}\text{-NCO})_2]$ (2), $[\text{Ni}_2(\text{L}^2)_2(\mu_{1,1}\text{-N}_3\text{O})_2] \cdot 2\text{CH}_3\text{CN}$ (3), $[\text{Ni}_2(\text{L}^2)_2(\mu_{1,1}\text{-NCO})_2]$ (4), $[\text{Ni}_2(\text{L}^3)_2(\mu_{1,1}\text{-NCO})_2]$ (5), $[\text{Ni}_2(\text{L}^4)_2(\mu_{1,1}\text{-NCO})_2]$ (6), $[\text{Ni}_2(\text{L}^5)_2(\mu_{1,1}\text{-NCO})_2]$ (7) and $[\text{Ni}_2(\text{L}^6)_2(\mu_{1,1}\text{-NCO})_2]$ (8) have been reported, and an emphasis was also given to establish magneto-structural correlation in these systems, that is yet to be established for cyanate-bridged Ni^{II} complexes. Moreover, the elaborated DFT study was performed for in-depth understanding of the magnetic interaction in these systems.

Experimental section

Materials and physical measurements

Chemicals such as nickel(II) nitrate hexahydrate, 2-hydroxy-3-methoxybenzaldehyde, 5-nitrosalicylaldehyde, 5-bromo-3-methoxysalicylaldehyde, 2-hydroxy-1-naphthaldehyde, 4-(diethylamino)salicylaldehyde and *N,N*-dimethylpropylenetriamine were commercially available reagent or analytical grade chemicals and used as received. 2-Hydroxy-3-methoxy-5-methylbenzaldehyde was synthesized following a literature



- HL¹: $\text{R}_1 = \text{OMe}$ and $\text{R}_2 = \text{Me}$
- HL²: $\text{R}_1 = \text{OMe}$ and $\text{R}_2 = \text{H}$
- HL³: $\text{R}_1 = \text{H}$ and $\text{R}_2 = \text{NO}_2$
- HL⁴: $\text{R}_1 = \text{H}$ and $\text{R}_2 = \text{Br}$
- HL⁵: $\text{R}_1 = \text{H}$ and $\text{R}_2 = \text{NET}_2$

Scheme 1 Drawing of the ligands used in the present study.



reported method.^{27,28} Solvents were of reagent grade and used without further purification.

Elemental analyses for carbon, hydrogen and nitrogen were carried out in a PerkinElmer 240C elemental analyser. FTIR spectra of the complexes in the range 4000 to 400 cm^{-1} were measured in a Thermo Scientific Nicolet iS5 FTIR spectrometer using a universal ATR sampling accessory. Direct current (dc) magnetic susceptibility measurements were performed on a Quantum Design MPMS-XL-5 magnetometer under a static magnetic field of 10 kOe in the temperature range of 2 to 300 K. The field dependent magnetization data were collected in the range of dc magnetic field 0–50 kOe at 5 K. All magnetic data were corrected for the sample holder and for the diamagnetic contribution of the samples.

Synthesis of Schiff base ligands HL^1 – HL^6

Ligands HL^1 – HL^6 were prepared adopting conventional Schiff base condensation method in which *N,N*-dimethyldipropylenetriamine was allowed to react with 2-hydroxy-3-methoxy-5-methylbenzaldehyde, 2-hydroxy-3-methoxybenzaldehyde, 5-nitrosalicylaldehyde, 5-bromo-3-methoxysalicylaldehyde, 2-hydroxy-1-naphthaldehyde or 4-(diethylamino)salicylaldehyde in methanol under reflux to afford tetradentate $\{\text{N}_3\text{O}\}$ donor Schiff base ligands HL^1 – HL^6 respectively. In a typical reaction, *N,N*-dimethyldipropylenetriamine (0.5 mmol, 80 mg) and 2-hydroxy-3-methoxy-5-methylbenzaldehyde (0.5 mmol, 83 mg) in 20 mL methanol were heated to reflux for *ca.* 1 h, and thereafter allowed to cool at room temperature. The dark-orange methanol solution of HL^1 was subsequently used for the synthesis of complexes **1** and **2**. Similarly, Schiff base ligands HL^2 – HL^6 were prepared, when condensation reactions were carried out using 2-hydroxy-3-methoxybenzaldehyde, 5-nitrosalicylaldehyde, 5-bromo-3-methoxysalicylaldehyde, 4-(diethylamino)salicylaldehyde or 2-hydroxy-1-naphthaldehyde in place of 2-hydroxy-3-methoxy-5-methylbenzaldehyde and afterward directly used for the synthesis of complexes **3**–**8**.

Synthesis of $[\text{Ni}_2(\text{L}^1)_2(\mu_{1,1}\text{-N}_3)_2]$ (1)

$\text{Ni}(\text{NO}_3)_2 \cdot 6\text{H}_2\text{O}$ (145 mg, 0.5 mmol), dissolved in 10 mL of methanol, was added to a 20 mL of methanol solution of Schiff base HL^1 (0.5 mmol) with stirring. A 10 mL methanol solution of sodium azide (NaN_3) (0.5 mmol, 33 mg) was added to the reaction mixture with constant stirring. The resulting dark-green solution was thereafter allowed to reflux for *ca.* 30 min. The reaction mixture was then filtered and kept at ambient temperature for slow evaporation. Crops of dark-green crystals, suitable for X-ray diffraction study, were developed over a period of one week. The crystals were filtered off and washed with cold methanol and dried in air to obtain analytically pure complex **1**. Yield: 175 mg (86%). Anal. calcd for $\text{C}_{34}\text{H}_{56}\text{N}_{12}\text{Ni}_2\text{O}_4$: C 50.15%, H 6.93%, N 20.64%. Found: C 50.34%, H 7.04%, N 20.47%. Selected FTIR bands (cm^{-1}): 1621 s ($\nu_{\text{C}=\text{N}}$); 2051 s ($\nu_{\text{N}_3^-}$); 3161 w ($\nu_{\text{N}-\text{H}}$); 1400–1610 cm^{-1} ($\nu_{\text{C}=\text{C}}$).

Synthesis of $[\text{Ni}_2(\text{L}^1)_2(\mu_{1,1}\text{-NCO})_2]$ (2)

Complex **2** was prepared adopting a very similar method as described for **1** with only exception that NaNCO was used in place of NaN_3 . Colour: dark-green. Yield: 141 mg (69%). Anal. calcd for $\text{C}_{36}\text{H}_{56}\text{N}_8\text{Ni}_2\text{O}_6$: C 53.10%, H 6.93%, N 13.76%. Found: C 53.24%, H 7.08%, N 13.52%. Selected FTIR bands (cm^{-1}): 1617 s ($\nu_{\text{C}=\text{N}}$); 2166 s (ν_{NCO}); 3155 w ($\nu_{\text{N}-\text{H}}$); 1405–1615 cm^{-1} ($\nu_{\text{C}=\text{C}}$).

Synthesis of $[\text{Ni}_2(\text{L}^2)_2(\mu_{1,1}\text{-N}_3)_2] \cdot 2\text{CH}_3\text{CN}$ (3)

Complex **3** was prepared applying a very similar methodology as described for **1**, but ligand HL^2 was used instead of ligand HL^1 and a methanol/acetonitrile (1 : 1, v/v) solvent mixture was used for the synthesis. Colour: dark-green. Yield: 180 mg (83%). Anal. calcd for $\text{C}_{36}\text{H}_{58}\text{N}_{14}\text{Ni}_2\text{O}_4$: C 49.80%, H 6.73%, N 22.58%. Found: C 49.94%, H 6.88%, N 22.37%. Selected FTIR bands (cm^{-1}): 1620 s ($\nu_{\text{C}=\text{N}}$); 2052 s ($\nu_{\text{N}_3^-}$); 3163 w ($\nu_{\text{N}-\text{H}}$); 1402–1610 cm^{-1} ($\nu_{\text{C}=\text{C}}$).

Synthesis of $[\text{Ni}_2(\text{L}^2)_2(\mu_{1,1}\text{-NCO})_2]$ (4)

Complex **4** was synthesised adopting the same methodology applied for the synthesis of **2**, but ligand HL^2 was used instead of ligand HL^1 . Colour: dark-green. Yield: 138 mg (70%). Anal. calcd for $\text{C}_{34}\text{H}_{52}\text{N}_8\text{Ni}_2\text{O}_6$: C 51.94%, H 6.67%, N 14.25%. Found: C 52.05%, H 6.69%, N 14.11%. Found: C 53.24%, H 7.08%, N 13.52%. Selected FTIR bands (cm^{-1}): 1624 s ($\nu_{\text{C}=\text{N}}$); 2171 s (ν_{NCO}); 3165 w ($\nu_{\text{N}-\text{H}}$); 1410–1615 cm^{-1} ($\nu_{\text{C}=\text{C}}$).

Synthesis of $[\text{Ni}_2(\text{L}^3)_2(\mu_{1,1}\text{-NCO})_2]$ (5)

Complex **5** was synthesised following an identical methodology that applied for the synthesis of **2**, but ligand HL^3 was used instead of ligand HL^1 . Colour: dark-green. Yield: 155 mg (76%). Anal. calcd for $\text{C}_{32}\text{H}_{46}\text{N}_{10}\text{Ni}_2\text{O}_8$: C 47.09%, H 5.68%, N 17.16%. Found: C 47.24%, H 5.78%, N 17.00%. Found: C 53.24%, H 7.08%, N 13.52%. Selected FTIR bands (cm^{-1}): 1301 s and 1594 m (ν_{NO_2}); 1624 m ($\nu_{\text{C}=\text{N}}$); 2173 s (ν_{NCO}); 3211 w ($\nu_{\text{N}-\text{H}}$); 1405–1610 cm^{-1} ($\nu_{\text{C}=\text{C}}$).

Synthesis of $[\text{Ni}_2(\text{L}^4)_2(\mu_{1,1}\text{-NCO})_2]$ (6)

Complex **6** was prepared following an identical procedure as described for **2** with only exception that ligand HL^4 was used in place of ligand HL^1 . Colour: dark-green. Yield: 194 mg (82%). Anal. calcd for $\text{C}_{68}\text{H}_{100}\text{Br}_4\text{N}_{16}\text{Ni}_4\text{O}_{12}$: C 43.26%, H 5.34%, N 11.87%. Found: C 43.01%, H 5.38%, N 11.72%. Selected FTIR bands (cm^{-1}): 1621 s ($\nu_{\text{C}=\text{N}}$); 2172 s (ν_{NCO}); 3172 w ($\nu_{\text{N}-\text{H}}$); 1400–1605 cm^{-1} ($\nu_{\text{C}=\text{C}}$).

Synthesis of $[\text{Ni}_2(\text{L}^5)_2(\mu_{1,1}\text{-NCO})_2]$ (7)

Complex **7** was prepared applying a very similar methodology as described for **2**, but ligand HL^5 was used instead of ligand HL^1 . Colour: dark-green. Yield: 122 mg (59%). Anal. calcd for $\text{C}_{40}\text{H}_{52}\text{N}_8\text{Ni}_2\text{O}_4$: C 58.14%, H 6.34%, N 13.56%. Found: C 57.81%, H 6.49%, N 13.37%. Selected FTIR bands (cm^{-1}): 1584 s ($\nu_{\text{C}=\text{N}}$); 2172 s (ν_{NCO}); 3134 w ($\nu_{\text{N}-\text{H}}$); 1410–1620 cm^{-1} ($\nu_{\text{C}=\text{C}}$).



Table 1 Crystallographic data and structural refinement parameters of 1–8

	1	2	3	4	5	6	7	8
Empirical formula	$C_{34}H_{56}N_{12}Ni_2O_4$	$C_{36}H_{56}N_8Ni_2O_6$	$C_{34}H_{58}N_{14}Ni_2O_4$	$C_{34}H_{52}N_8Ni_2O_6$	$C_{32}H_{46}N_{10}Ni_2O_8$	$C_{68}H_{100}Br_4N_{16}Ni_4O_{12}$	$C_{40}H_{52}N_8Ni_2O_4$	$C_{40}H_{66}N_{10}Ni_2O_4$
Formula weight (g mol ⁻¹)	814.32	814.30	868.38	786.25	816.21	188.11	826.31	868.44
Temperature (K)	150	150	298	150	150	150	150	150
Crystal system	Monoclinic	Monoclinic	Monoclinic	Monoclinic	Monoclinic	Monoclinic	Monoclinic	Monoclinic
Space group	$P2_1/n$	$P2_1/c$	$P2_1/c$	$P2_1/c$	$P2_1/c$	$P2_1/c$	$P2_1/n$	$P2_1/c$
<i>a</i> (Å)	14.9397(9)	11.0841(5)	11.8236(3)	10.4277(8)	11.489(4)	22.299(4)	9.2184(7)	14.1830(7)
<i>b</i> (Å)	16.9091(9)	14.7030(7)	18.2885(4)	19.5733(14)	15.3326(10)	19.031(3)	18.3850(12)	10.8572(5)
<i>c</i> (Å)	15.1735(9)	11.4961(5)	10.8047(2)	18.0962(13)	10.892(4)	9.0106(17)	11.5306(7)	15.1649(7)
α (deg)	90	90	90	90	90	90	90	90
β (deg)	91.850(2)	95.432(2)	115.053(1)	95.491(2)	108.741(11)	93.165(7)	96.090(3)	112.574(2)
γ (deg)	90	90	90	90	90	90	90	90
Volume (Å ³)	1865.10(15)	2116.55(8)	3676.6(5)	1764.8(10)	3818.1(12)	1943.2(2)	2085.1(3)	2085.1(3)
<i>Z</i>	4	4	4	4	2	2	2	2
D_{calc} (g cm ⁻³)	1.412	1.450	1.363	1.420	1.536	1.642	1.142	1.338
μ (mm ⁻¹)	1.037	1.066	0.944	1.079	1.132	3.134	1.021	0.924
$F(000)$	1728	864	920	1664	856	1936	872	928
θ range (deg)	1.804–27.132	1.846–26.393	1.90–27.60	2.221–29.123	1.872–28.122	1.829–26.679	2.222–29.186	2.374–27.152
Reflections collected	37 738	18 195	34 956	35 838	18 536	95 335	20 183	4829
Independent reflections (R_{int})	8448 (0.0603)	3821 (0.0722)	4895 (0.0303)	9861 (0.0757)	4254 (0.0621)	7898 (0.0678)	5231 (0.0468)	4829 (0.0600)
Observed reflections [$I > 2\sigma(I)$]	6049	2669	4171	6450	3282	6651	3912	4113
Restraints/parameters	1/485	1/253	0/260	0/476	0/241	0/483	0/250	0/262
Goodness-of-fit on F^2	1.004	1.021	1.050	1.038	1.022	1.161	1.089	1.045
Final <i>R</i> indices [$I > 2\sigma(I)$]	$R_1 = 0.0423$	$R_1 = 0.0391$	$R_1 = 0.0286$	$R_1 = 0.0456$	$R_1 = 0.0384$	$R_1 = 0.0484$	$R_1 = 0.0453$	$R_1 = 0.0334$
<i>R</i> Indices (all data)	$wR_2 = 0.0994$	$wR_2 = 0.0805$	$wR_2 = 0.0705$	$wR_2 = 0.0913$	$wR_2 = 0.0755$	$wR_2 = 0.1323$	$wR_2 = 0.0881$	$wR_2 = 0.0823$
Largest diff. peak/hole (e Å ⁻³)	0.9671–0.562	$wR_2 = 0.1123$	$wR_2 = 0.0935$	$wR_2 = 0.0758$	$wR_2 = 0.1080$	$wR_2 = 0.1380$	$wR_2 = 0.0966$	$wR_2 = 0.0878$
		0.384/–0.386	0.490/–0.222	0.837/–0.625	0.383/–0.460	1.178/–1.035	0.348/–0.342	0.342/–0.386

Synthesis of $[\text{Ni}_2(\text{L}^6)_2(\mu_{1,1}\text{-NCO})_2]$ (8)

Complex **8** was synthesised adopting the same methodology applied for the synthesis of **2**, but ligand HL^6 was used instead of ligand HL^1 . Colour: dark-green. Yield: 132 mg (61%). Anal. calcd for $\text{C}_{40}\text{H}_{66}\text{N}_{10}\text{Ni}_2\text{O}_4$: C 55.32%, H 7.66%, N 16.13%. Found: C 55.24%, H 7.89%, N 15.81%. Selected FTIR bands (cm^{-1}): 1613 s ($\nu_{\text{C}=\text{N}}$); 2173 s (ν_{NCO}); 3166 w ($\nu_{\text{N-H}}$); 1400–1600 cm^{-1} ($\nu_{\text{C=C}}$).

X-ray crystallography

Single crystal X-ray diffraction data of complexes **1–8** were collected on a Bruker Kappa Apex-II CCD diffractometer equipped with a fine focus sealed tube of monochromated Mo-K α radiation ($\lambda = 0.71073 \text{ \AA}$). The collected data frames were processed with SAINT-plus programme, and finally the intensity data were corrected by applying multi-scan absorption correction method implemented in SADABS programme.²⁹ The structures were solved by the direct method (SHELXS) and refined by full-matrix least squares technique based on F^2 using SHELX-2018 programme.³⁰ All the non-hydrogen atoms were refined with anisotropic thermal parameters. Whereas hydrogen atoms attached to carbon atoms were included in geometrically idealised positions and refined with a fixed thermal parameter (1.2 or 1.5 times) with respect to their parent atoms, the secondary amine protons were located on the difference Fourier map and refined freely. Other details of crystallographic data and structure refinement parameters are placed in Table 1. Crystal structures were generated through the programme MERCURY-4.3.1 and POV-ray software.

Results and discussion

Syntheses and general characterization

Tetradeятate $\{\text{N}_3\text{O}\}$ -donor Schiff base ligands ($\text{HL}^1\text{--HL}^6$) were synthesised by condensation reaction of *N,N*-dimethylpropyleneetriamine with 2-hydroxy-3-methoxy-5-methylbenzaldehyde, 2-hydroxy-3-methoxybenzaldehyde, 5-nitrosalicylaldehyde, 5-bromo-3-methoxysalicylaldehyde, 4-(diethylamino)salicylaldehyde or 2-hydroxy-1-naphthaldehyde in methanol, respectively (Scheme 1). Thereafter, eight new dark-green binuclear pseudohalide-bridged complexes, $[\text{Ni}_2(\text{L}^1)_2(\mu_{1,1}\text{-N}_3)_2]$ (**1**), $[\text{Ni}_2(\text{L}^1)_2(\mu_{1,1}\text{-NCO})_2]$ (**2**), $[\text{Ni}_2(\text{L}^2)_2(\mu_{1,1}\text{-N}_3)_2 \cdot 2\text{CH}_3\text{CN}$ (**3**), $[\text{Ni}_2(\text{L}^2)_2(\mu_{1,1}\text{-NCO})_2]$ (**4**), $[\text{Ni}_2(\text{L}^3)_2(\mu_{1,1}\text{-NCO})_2]$ (**5**), $[\text{Ni}_2(\text{L}^4)_2(\mu_{1,1}\text{-NCO})_2]$ (**6**), $[\text{Ni}_2(\text{L}^5)_2(\mu_{1,1}\text{-NCO})_2]$ (**7**) and $[\text{Ni}_2(\text{L}^6)_2(\mu_{1,1}\text{-NCO})_2]$ (**8**) were resynthesized in high yield through one-pot reaction of *in situ* generated Schiff base ligand, $\text{Ni}(\text{NO}_3)_2 \cdot 6\text{H}_2\text{O}$ and pseudohalide salts in a 1:1:1 molar ratio in presence of triethylamine base in methanol or methanol/acetonitrile under reflux. All the compounds were routinely characterised by elemental analysis and IR spectroscopy.

The IR spectra of all the complexes (Fig. S1†) disclose characteristic azomethine $\text{C}=\text{N}$ stretching bond of the Schiff base ligands in the range 1584–1624 cm^{-1} . All of them also consist of N–H stretching band of the secondary amine group of the Schiff base ligands in the range 3134–3211 cm^{-1} . Most importantly, the IR spectra of complexes **1** and **3** display a very strong absorption band at around 2052 cm^{-1} which is attributed to the

asymmetric stretching frequency of azide ion, which is consistent with EO azide-bridged Ni^{II} systems. Similarly, IR bands for the asymmetric stretching vibrations of EO cyanate bridges in complexes **2**, **4–8** were observed in the range 2166–2173 cm^{-1} , which are usual for EO cyanate-bridges. Moreover, broadening/bifurcation of the stretching band of cyanate group in **2** and **6** is consistent with the presence of two crystallographically independent complex molecules (*vide infra*). The stretching frequency in the range of 1400–1620 cm^{-1} are assigned to phenyl (C=C) ring stretching for all the complexes. Additional bands at 1301 and 1594 cm^{-1} in **5** have been assigned to symmetric and asymmetric stretching vibrations of nitro group of the Schiff base ligand, respectively.

Description of crystal structures

X-ray crystallography reveals that all the complexes are isostructural with formulas $[\text{Ni}_2(\text{L}^1)_2(\mu_{1,1}\text{-N}_3)_2]$ (**1**), $[\text{Ni}_2(\text{L}^1)_2(\mu_{1,1}\text{-NCO})_2]$ (**2**), $[\text{Ni}_2(\text{L}^2)_2(\mu_{1,1}\text{-N}_3)_2 \cdot 2\text{CH}_3\text{CN}$ (**3**), $[\text{Ni}_2(\text{L}^2)_2(\mu_{1,1}\text{-NCO})_2]$ (**4**), $[\text{Ni}_2(\text{L}^3)_2(\mu_{1,1}\text{-NCO})_2]$ (**5**), $[\text{Ni}_2(\text{L}^4)_2(\mu_{1,1}\text{-NCO})_2]$ (**6**), $[\text{Ni}_2(\text{L}^5)_2(\mu_{1,1}\text{-NCO})_2]$ (**7**) and $[\text{Ni}_2(\text{L}^6)_2(\mu_{1,1}\text{-NCO})_2]$ (**8**), and they crystallized uniformly in the monoclinic unit cell but in either space group $P2_1/n$ (**1** and **7**) or $P2_1/c$ (**2–6** and **8**). The structures of all the complexes are eventually similar in that the neutral dinuclear complex molecules are constructed by doubly EO bridged N_3^- ions in **1** and **3** (Fig. 1) and NCO^- ions in **2** and **4–8** (Fig. 2). Whereas a full set of dinuclear complex molecule in **1** and two halves of the crystallographically independent centrosymmetrical dinuclear complex molecules in **2** and **6** are present in the asymmetric units, only a half of the centrosymmetrical dinuclear complex molecule constitutes the asymmetric units of **4**, **5**, **7** and **8**. Additionally, only in **3**, the complex molecules crystallized with acetonitrile solvent molecules. However, in all the complexes, the Ni^{II} centres are hexacoordinate with a distorted octahedral geometry in which each of the Ni^{II} ion is surrounded by three N donor atoms and one phenolate-O atom of the deprotonated Schiff base ligands and two N-atoms either from the EO bridging azide ions (in **1** and **3**) or cyanate ions (in **2** and **4–8**). The EO bridging pseudohalide ions share the common edges, leading to the edged-sharing bi-octahedral structures (see Fig. 1 and 2). In all these complexes, three N-atoms (imine, secondary amine and tertiary amine N-atoms) from the triamine part of the deprotonated Schiff base ligands coordinate the Ni^{II} centres in a facial configuration. The Ni–N bond lengths of imine, secondary amine and tertiary amine of the Schiff base ligands span in the range 2.046(2) to 2.239(2) \AA in **1–8**, which are comparable to those found in closely related Ni^{II} complexes reported in the literature (Table 2).^{17–23,31–51} The central $\{\text{Ni}_2\text{Ni}\}$ core in **1** and **3** is planar with the metal–metal separation and the Ni–N–Ni bridging angles are 3.355(1) and 3.374(1) \AA , and 101.00(8)°–101.99(8)°, respectively. Similarly, the metal–metal separations (3.327(1)–3.235(1) \AA) in the central $\{\text{Ni}_2\text{Ni}\}$ core structures in **2–8** are very similar as that found in **1** and **3**, but the Ni–N–Ni bridging angles in the range 96.79(9)–99.87(8)° are slightly lower than that found in **1** and **3**. The bridging region is slightly asymmetric as can be seen from the Ni–N bond distances of 2.120(2)–2.148(1) (shorter) and 2.197(2)–2.212(2) \AA (longer) of



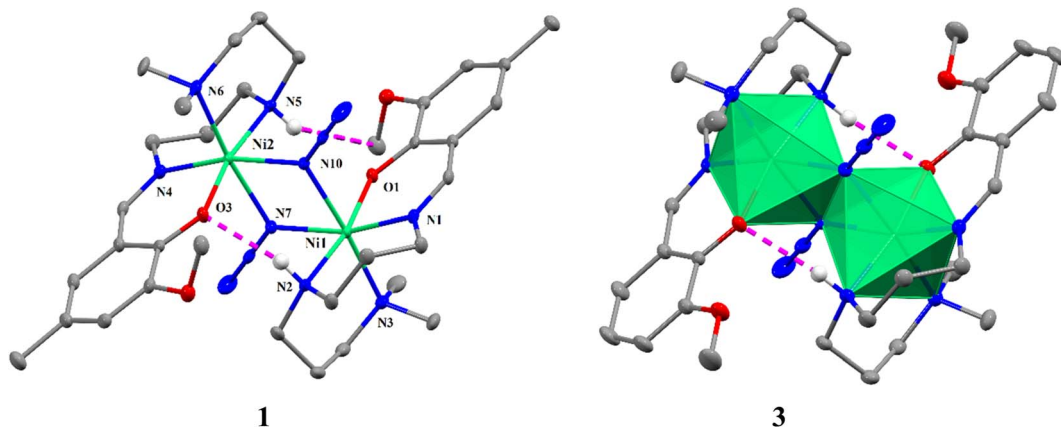


Fig. 1 Crystal structures of doubly $\mu_{1,1}$ -azido-bridged dinuclear Ni^{II} complexes **1** and **3** showing selected atom numbering scheme (left) and local polyhedral around Ni^{II} centre (right). Ellipsoids are drawn at the 30% probability level. The intramolecular H-bonds are shown as dashed lines.

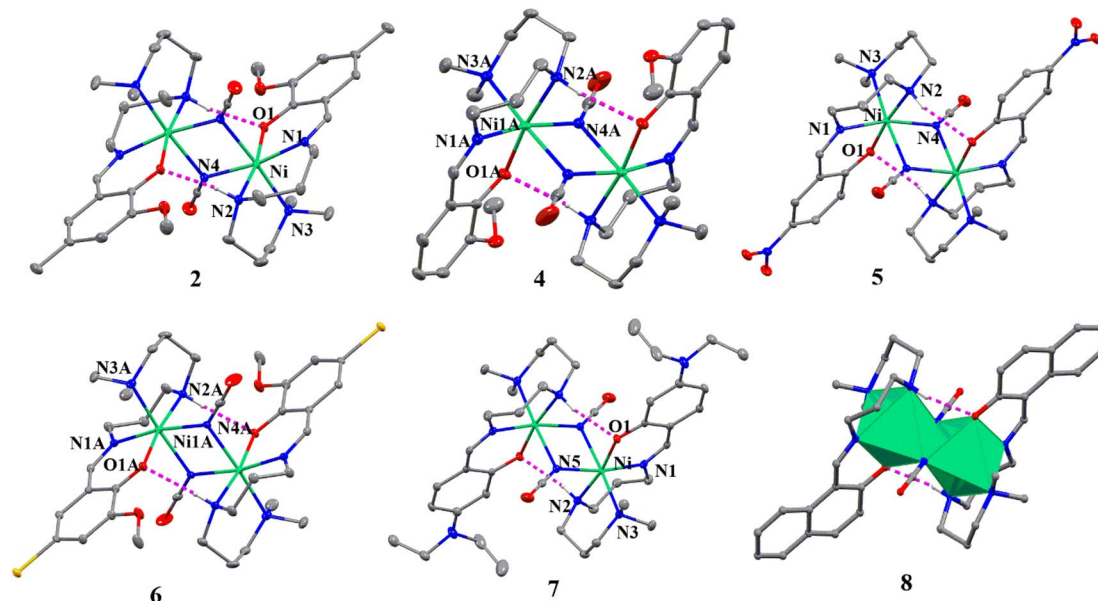


Fig. 2 Crystal structures of dinuclear Ni^{II} complexes **2** and **4–8** with selected atom numbering scheme. Ellipsoids are drawn at the 30% probability level. Hydrogen atoms are omitted for clarity of the picture. The noncovalent interactions are shown as dashed lines.

the bridging azide ions in **1** and **3** and two sets the $\text{Ni}-\text{N}$ bond distances ($2.091(4)$ – $2.134(2)$ Å and $2.221(4)$ – $2.2650(18)$ Å) of the bridging cyanate ions in **2**–**8**. Invariably, in these complexes, secondary amine hydrogen atom establishes moderately strong intramolecular hydrogen bonding interactions with the phenolate oxygen atom within the dinuclear unit with the donor-acceptor distances varying in the range 2.914 – 3.099 Å, to provide the solid-state stability of these compounds. Additional stability in the solid state is appeared from the different weak intermolecular interactions, such as $\text{C}-\text{H}\cdots\text{N}/\text{O}$, $\pi\cdots\pi$ and $\text{C}-\text{H}\cdots\pi$ in these complexes (Fig. S2–S9†).

Magnetic studies

The temperature dependence of direct current (dc) magnetic susceptibility measurements was carried out on crystalline

samples of **1**–**8** in the temperature range 2 – 300 K under a constant applied dc field of 10 kOe and the magnetic data were plotted as a function of χT vs. T (Fig. 3 and 4; χ being the molar magnetic susceptibility per dimer), while the molar magnetization as a function of applied dc magnetic field (M/μ_{B} per f.u. vs. H) for these complexes are depicted in Fig. S10.† At room temperature, the χT values are in most cases slightly higher than the theoretical value of 2.0 emu mol^{-1} K for two non-interacting Ni^{II} ions with $S = 1$ and $g = 2$, consistent with the presence of spin-orbit coupling in the Ni^{II} ion. As the temperature is lowered, the χT products increase continuously with decreasing temperature to attain maxima in all the cases and thereafter decrease sharply until 2 K. The magnetic behaviour of these samples is typical for an intramolecular ferromagnetic interaction between two Ni^{II} ions together with the influence of



Table 2 Selected bond lengths in Å for 1–8

Bond	1	2	3	4	5	6	7	8
Ni ^{II} –N (imine)	2.050(2) 2.046(2)	2.068(2)	2.060(1)	2.059(2) 2.066(2)	2.077(2)	2.075(4) 2.059(4)	2.059(2)	2.052(2)
Ni ^{II} –N (secondary amine)	2.109(2) 2.109(2)	2.106(2)	2.123(1)	2.117(2) 2.107(2)	2.102(2)	2.124(4) 2.117(4)	2.122(2)	2.113(2)
Ni ^{II} –N (tertiary amine)	2.198(2) 2.202(2)	2.233(2)	2.148(1)	2.239(2) 2.189(2)	2.205(2)	2.225(4) 2.227(4)	2.225(2)	2.202(2)
Ni ^{II} –O (phenolate)	2.002(2) 2.005(2)	1.992(2)	2.013(1)	2.001(2) 2.001(2)	2.069(2)	2.020(3) 2.011(3)	2.003(1)	2.003(2)
Ni ^{II} –N (pseudohalide)	2.136(2) 2.212(2) 2.197(2) 2.120(2)	2.134(2) 2.223(2)	2.148(1) 2.209(1)	2.114(2) 2.248(2) 2.115(2) 2.240(2)	2.101(2) 2.243(2)	2.118(4) 2.221(4) 2.091(4) 2.235(4)	2.114(2) 2.265(2)	2.112(2) 2.247(2)
Ni···Ni	3.355(1)	3.258(1)	3.374(1)	3.286(1) 3.298(1)	3.327(1)	3.299(1) 3.235(1)	3.292(1)	3.292(1)
Ni–N–Ni bridging angle	101.00(8) 101.99(8)	96.79(9)	101.48(5)	98.23(8)	99.87(8)	99.0(2) 97.93(8)	97.43(7)	98.04(7)

intermolecular interactions and/or zero-field splitting (ZFS) of ground state ($S = 2$), particularly at lower temperature. The saturation magnetization values of about $4 M/\mu_B$ per f.u. also suggest the ferromagnetic interaction between the Ni^{II} centres, leading to the $S = 2$ ground state in these systems. Therefore, the magnetic susceptibility data can nicely be modelled with a full-matrix diagonalisation approach assuming an isotropic spin exchange Hamiltonian ($-2J\hat{S}_1 \cdot \hat{S}_2$), Zeeman interaction (g_{Ni} , average) and zero-field splitting (D)/intermolecular interaction (zJ') to extract the different numerical parameters using the PHI programme.⁵² The best fittings of the magnetic data yielded $J = +36.8(5) \text{ cm}^{-1}$, $g_{Ni} = 2.14(1)$, and $D = +7.79(4) \text{ cm}^{-1}$ for complex **1** and $J = +34.48(2) \text{ cm}^{-1}$, $g_{Ni} = 2.07(1)$ and $D = +13.61(1) \text{ cm}^{-1}$ for complex **3**, while the numerical parameters for complexes **2** and **4–8** are assembled in Table 3.

It is now well studied that the sign and magnitude of the exchange interaction (J) among the paramagnetic centres is governed by several structural parameters in which the bridging angle plays the most important role in determining the sign and

strength of magnetic interactions. The extensive theoretical works by Ruiz *et al.*²⁴ showed that the doubly $\mu_{1,1}$ -azido-bridged dinuclear Ni^{II} systems experience ferromagnetic interactions through the bridging Ni–N–Ni angles (θ) studied in between 80° and 115° in which J value increases with increasing angles and reaches the maximum at around 104° , and thereafter decreases with increasing θ . Interestingly, all the reported $\mu_{1,1}$ -azido-bridged dinuclear Ni^{II} systems exhibit ferromagnetic interactions with only one exception where a very low bridging angle of 90.4° mediates the antiferromagnetic interaction between Ni^{II} centres.³⁷ The Ni–N–Ni bridging angles found in **1** and **3** are comparable ($101.00(8)^\circ$ and $101.99(8)^\circ$ for **1** and $101.48(5)^\circ$ for **3**), and are close to the angle where the strong ferromagnetic interaction is expected between two Ni^{II} ions as shown in the theoretical study,^{24,53} and thus moderately strong J values ($36.8(5)$ and $34.48(2) \text{ cm}^{-1}$ for **1** and **3**, respectively) found in these systems are in good agreement with the theoretical calculations. However, unlike theoretical prediction, a large number of magnetically characterized $\mu_{1,1}$ -azido-bridged

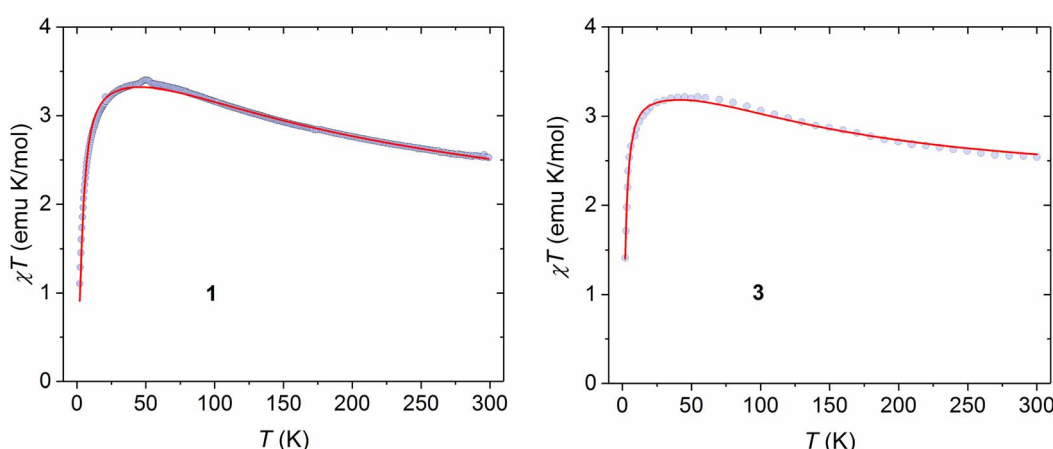


Fig. 3 Temperature dependence of χT products measured at 10 kOe dc field for **1** and **3**. Symbols and solid lines represent experimental and best fitted data.



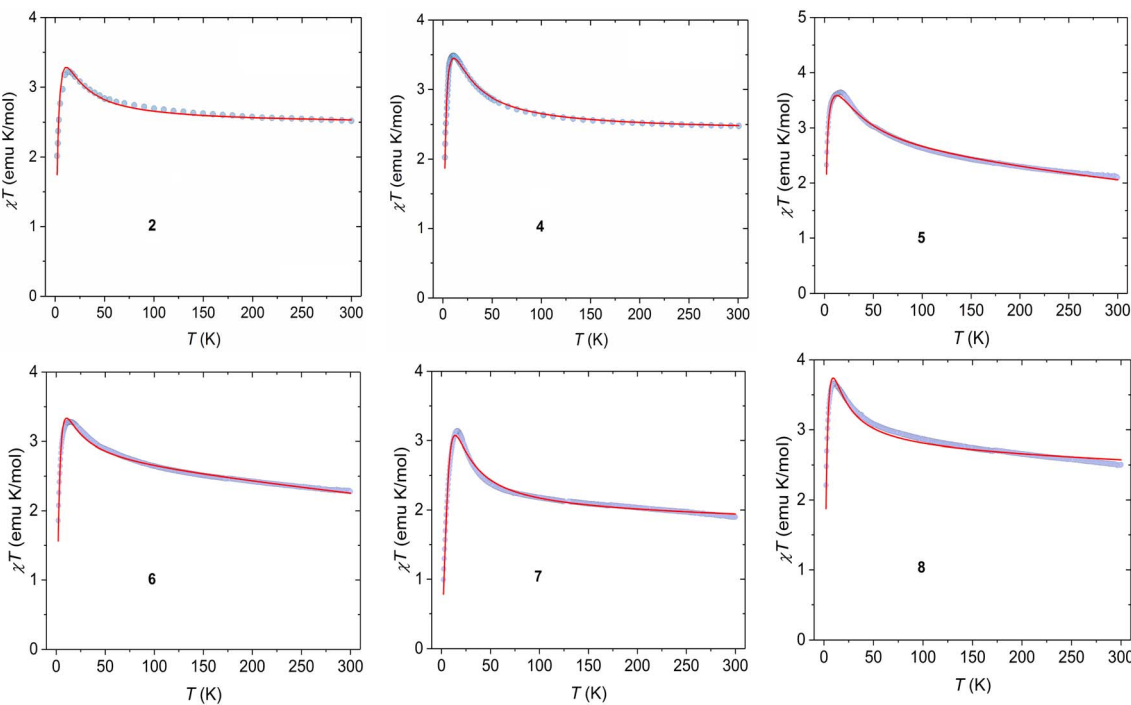


Fig. 4 Temperature dependence of χT products measured at 10 kOe dc field for 2 and 4–8. Symbols and solid lines represent experimental and best fitted data.

Table 3 Selected structural and magnetic data of doubly end-on cyanato bridged Ni^{II} dimers (following $\hat{H} = -2J\hat{S}_1\cdot\hat{S}_2$ convention)^a

Compounds	J (cm ⁻¹)	D (cm ⁻¹)	g	M–N (Å)	M–N–M (°)	Dihedral angles (°) between two Ni1–Ni2–N _b –X _t planes ^b	Ref.
2	+4.17(8)	+9.11(2)	2.22(1)	2.134, 2.223	96.79(9)	158.05	This work
4	+5.75(3)	+10.80(2)	2.18(1)	2.114, 2.248 2.115, 2.240	98.23(8) 97.93(8)	174.77 162.72	This work
5	+7.80(9)	+2.00(3)	2.238(2)	2.101, 2.243	99.87(8)	168.46	This work
6	+9.1(1)	+2.84(2)	2.141(2)	2.118, 2.221 2.091, 2.235	99.0(2) 96.8(2)	165.25 177.81	This work
7	+4.6(2)	+7.63(7)	1.973(6)	2.114, 2.265	97.43(7)	178.98	This work
8	+4.7(2)	+2.34(2)	2.315(7)	2.112, 2.247	98.04(7)	174.55	This work
$[\text{Ni}_2(\text{L}^9)_2(\mu_{1,1}\text{-NCO})_2](\text{ClO}_4)_2$	+1.7	+3.6	2.23	2.125, 2.090	94.4, 95.8	177.86	19
$[\text{Ni}_2(\text{L}^{10})_2(\mu_{1,1}\text{-NCO})_2](\text{ClO}_4)_2$	+2.8	+3.6	2.23	2.099, 2.115	95.33, 95.79	175.41	19
$[\text{Ni}_2(\text{terpy})_2(\mu_{1,1}\text{-NCO})_2(\text{H}_2\text{O})_2](\text{PF}_6)_2$	+4.59	-12.32	2.23	2.044, 2.195	97.7	175.10	20
$[\text{Ni}_2(\text{L}^{11})_2(\mu_{1,1}\text{-NCO})_2]$	+6.85	+7.18	2.19	2.107, 2.244 2.115, 2.280	97.84, 98.74	171.68	21
$[\text{Ni}_2(\text{L}^{12})_2(\mu_{1,1}\text{-NCO})_2]$	+5.31	+5.00	2.19	2.225, 2.201	98.47	172.73	22
$[\text{Ni}_2(\text{L}^{13})_2(\mu_{1,1}\text{-NCO})_2]$	+3.70	+8.05	2.28	2.119, 2.205	97.45, 97.84	172.94	23

^a $\text{L}^9 = [\text{N,N-bis}(2\text{-pyridinylmethylene})\text{propane-1,3-diamine}$; $\text{L}^{10} = \text{N,N-bis}(\text{pyridin-2-yl})\text{benzylideneethane-1,2-diamine}$; terpy = terpyridine; L^{10} , L^{11} and L^{12} = tetradeятate N_3O donor Schiff base ligands. ^b As defined in the text and average values are reported.

dinuclear Ni^{II} systems do not display a clear relationship of J values with the Ni–N–Ni bridging angles as a small variation of the Ni–N–Ni angles in a narrow range of 98° – 103.9° display a wide range of J values from 1.91 to 43.9 cm⁻¹.^{31–51} This can be further confirmed by the fact that the present bridging angles of $101.00(8)^\circ$ and $101.99(8)^\circ$ for **1** and $101.48(5)^\circ$ for **3** are comparable to the value of 101.0° in $[\text{Ni}_2(\text{L}^7)_2(\mu_{1,1}\text{-N}_3)_2(\text{N}_3)_2](\text{L}^7 = \text{a tridentate quinoline-based ligand})$ ⁴⁰ and 101.79° (average

angle) in $[\text{Ni}_2(\text{L}^8)_2(\text{N}_3)_2(\mu_{1,1}\text{-N}_3)_2]\cdot\text{CH}_3\text{OH}$ ($\text{L}^8 = \text{N,N-dimethyl-N'-(pyrid-2-ylmethyl)-ethylenediamine}$),⁵⁴ yet they display significantly different J values of 6.1 and 1.91 cm⁻¹, respectively. In contrast, the magnetic coupling constants of the present systems are nicely matched with other reported compound $[\text{Ni}(\text{pepsi})(\mu_{1,1}\text{-N}_3)_2]_2$ (where pepsi = $\text{N}'\text{-}(2\text{-pyridin-2-ylethyl})\text{pyridine-2-carbaldimine}$)⁴⁷ that displayed very similar bridging angle of 101.6° with J value of 36.3 cm⁻¹. Moreover, the present J



values are significantly different from our previous report with similar ligand system, derived from the condensation of salicylaldehyde and *N,N*-dimethylpropylenetriamine, in which J value and average bridging angle are found to be 10 cm^{-1} and 101.35° , respectively.

In contrast to extensively rich magneto-structurally characterized $\mu_{1,1}\text{-N}_3$ bridged Ni^{II} systems, only few doubly $\mu_{1,1}\text{-NCO}$ bridged dinuclear Ni^{II} complexes are available in the literature.^{19–23} Therefore, the addition of six new examples in this series enriches the field of doubly $\mu_{1,1}\text{-NCO}$ bridged dinuclear Ni^{II} compounds. As can be seen from Table 3 that the magnetic coupling constants are weak compared to azide-bridged systems, which is because of the presence of polarizable π systems and two different N and O donor atoms in cyanate ion, rendering to be a poor magnetic coupler in comparison to azide analogue. The magnetic and relevant

crystallographic data of all doubly $\mu_{1,1}\text{-NCO}$ bridged dinuclear Ni^{II} systems as given in Table 3 show the variation of J values in a narrow range of $1.7\text{--}9.1\text{ cm}^{-1}$.^{19–23} Remarkably, unlike azide-bridged systems, the cyanate analogues follow a general trend in which J value increases with increase in bridging angles (Fig. 5, left), similar to theoretical prediction that has been conducted by Ruiz *et al.* for azide analogues.²⁴ The possibility of more precise correlation cannot be ruled out if simultaneous influence of different structural parameters take into account in correlation studies. For example, other than the bridging angle, the deviation of the bridging azide or cyanate ligand from Ni_2N_2 plane could influence the magnetic interaction between the paramagnetic centres as with increase in deviation from Ni_2N_2 plane orbitals overlap is expected to be reduced, leading to a weaker magnetic coupling *via* super-exchange mechanism. Although a great correlation is not observed when experimental

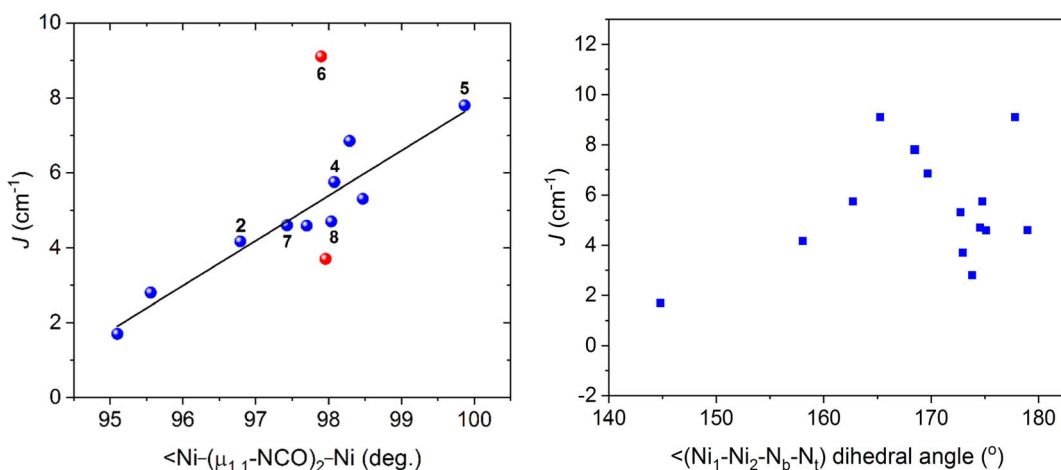


Fig. 5 Magneto-structural correlation data showing dependence of J values with $\text{Ni}-(\mu_{1,1}\text{-NCO})_2\text{-Ni}$ bridging angles. The red symbols indicates that these data have been excluded from this correlation. The data have been taken from Table 3 and the data of the present work are denoted by numbers.

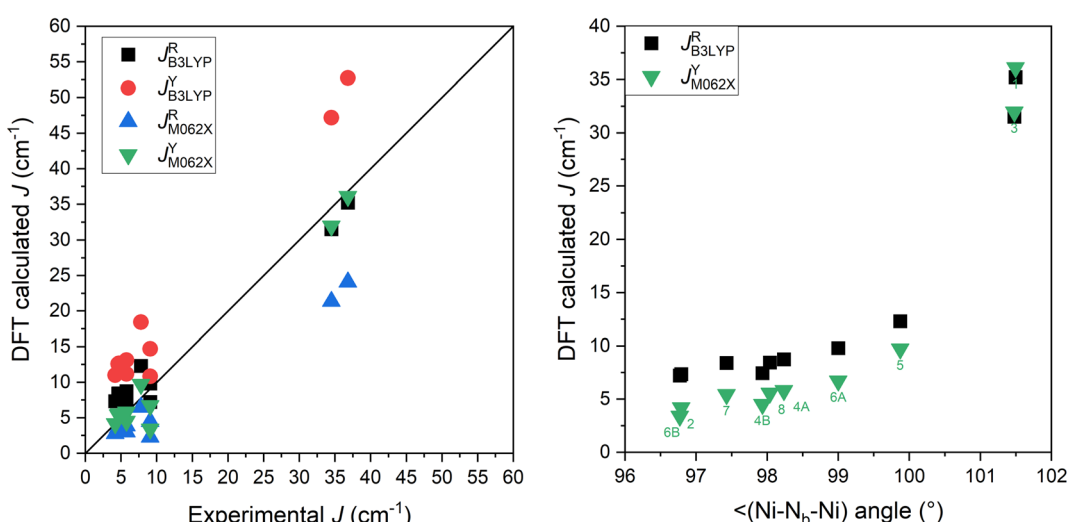


Fig. 6 The comparison of DFT calculated and experimental values of J in complexes 1–8 (left). The $\text{Ni}-\text{N}_b\text{-Ni}$ angle dependence of selected DFT J -values: J_{B3LYP}^R and J_{M062X}^Y (right).



J values are plotted as a function of Ni1–Ni2–N_b–X_t dihedral angles (N_b and X_t are bridging N and terminal N or O atom of bridging ligands, respectively) (Fig. 5, right), the increasing trend of J values with dihedral angles could not be ruled out, further confirming that the simultaneous influence of different structural parameters are involved in magnetic communication.

Theoretical calculations

The variation of the magnetic interaction in presented cyanate and azide bridged Ni^{II} complexes motivated us to investigate these molecular systems thoroughly by the Density Functional Theory (DFT) using freely available ORCA 5.0 software.⁵⁵ The isotropic exchange interaction J is usually calculated with the help of the broken-symmetry DFT calculations by comparing the energies of the high-spin (HS, $\uparrow\uparrow$) and broken-symmetry spin states (BS, $\uparrow\downarrow$), $\Delta = \varepsilon_{\text{BS}} - \varepsilon_{\text{HS}}$. The Δ -parameter is then used to calculate J with the help of Ruiz⁵⁶ or Yamaguchi⁵⁷ formulas:

$$J^R = \Delta / [(S_1 + S_2)(S_1 + S_2 + 1)]$$

$$J^Y = \Delta / [\langle S^2 \rangle_{\text{HS}} - \langle S^2 \rangle_{\text{BS}}]$$

herein, we decided to apply two DFT functionals, namely well-known B3LYP hybrid functional⁵⁸ and M06-2X hybrid meta-GGA functional.⁵⁹ First one provided good performance for many polynuclear 3d-metal complexes,⁶⁰ while the second functional was benchmarked as one of the best for thiocyanate and cyanate double bridged binuclear Ni^{II} complexes.⁶¹ All calculations were performed with ZORA relativistic approximation⁶² and relativistic analogues of Ahlrichs basis sets,⁶³ ZORA-def2-TZVP for Ni, ZORA-def2-TZVP(-f) for all non-metals except for C and H for which ZORA-def2-SVP was used. First, dinuclear molecular fragments of **1–8** were extracted from experimental X-ray data while the positions of the hydrogen atoms were normalized with the help of Mercury software.⁶⁴ The respective results of DFT calculations are presented in Fig. 6 and Table S1† as J_{B3LYP}^R , J_{B3LYP}^Y , J_{M062X}^R and J_{M062X}^Y . It is evident that the best match with the experimental J -parameters were

achieved for J_{B3LYP}^R and J_{M062X}^Y and both approaches provided similar results as is also depicted in Fig. 6 (right) for Ni–N_b–Ni angle dependence, where N_b is the bridging atom of N₃ or NCO ligand.

As discussed in previous section, the Ni–N_b–Ni angle is not unique parameter to evaluate the magnetic interactions in these dinuclear complexes. Indeed, the search in the Cambridge Crystallographic Database (CSD)⁶⁵ revealed not only large deviation of Ni–N_b–Ni angle in azido and cyanate bridged complexes, but also the significant span of dihedral angles defined as Ni1–Ni2–N_b–X_t, where X_t is terminal atom of pseudo-halide ligand (X_t is N for azide and O for cyanate) – Fig. S11 and S12.† This inspired us to further explore the magneto-structural correlation in simple model compounds $[\text{Ni}_2(\mu_{1,1}-\text{N}_3)_2(\text{NH}_3)_8]^{2+}$ and $[\text{Ni}_2(\mu_{1,1}-\text{NCO})_2(\text{NH}_3)_8]^{2+}$ – Fig. 7. The good performance of M06-2X functional motivated us to use it both for geometry optimization and calculations of J_{M062X}^Y . First, we studied dependence of J on Ni–N_b–Ni angle ranging from 75 to 115° without restricting dihedral angles (Fig. 8 left, empty symbols).

It was found that dihedral angles Ni1–Ni2–N_b–X_t can reach values down to ~100° (the optimized molecular geometries are provided as XYZ coordinates in ES†). These calculations showed that strongest ferromagnetic exchange is provided for Ni–N_b–Ni angles close to 100° and that stronger ferromagnetic exchange is induced by N₃ ligand. For Ni–N_b–Ni angles below ~90°, the antiferromagnetic exchange is expected. Second, the dihedral angles Ni1–Ni2–N_b–X_t were fixed to value 180° and again Ni–N_b–Ni angle was varied similarly to previous case. Interestingly, it led to dramatic threefold increase of the ferromagnetic exchange for N₃-bridged complexes reaching value up to $J = 28 \text{ cm}^{-1}$ for Ni–N_b–Ni angle equal to 100°. In case of NCO-bridged complexes twofold increase was observed (Fig. 8 left, full symbols). Finally, the impact of dihedral angle is demonstrated in Fig. 8 (right), where the computational protocol was applied for fixed Ni–N_b–Ni = 100° and variation of dihedral angle resulted in consequential changes of the isotropic exchange.

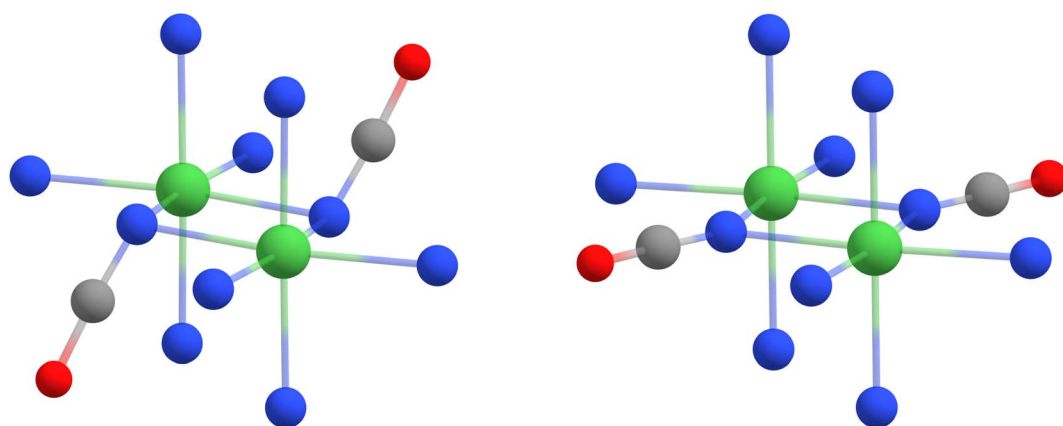


Fig. 7 The comparison of DFT geometries using M06-2X functional obtained for model complex $[\text{Ni}_2(\mu_{1,1}-\text{NCO})_2(\text{NH}_3)_8]^{2+}$ for Ni–N_b–Ni bond angles equal to 100° (left) and similar calculation in which Ni1–Ni2–N_b–X_t dihedral angles were fixed to 180° (right). The nickel atoms are green, nitrogen atoms are blue, carbon atoms are grey, and the hydrogen atoms were omitted for clarity.



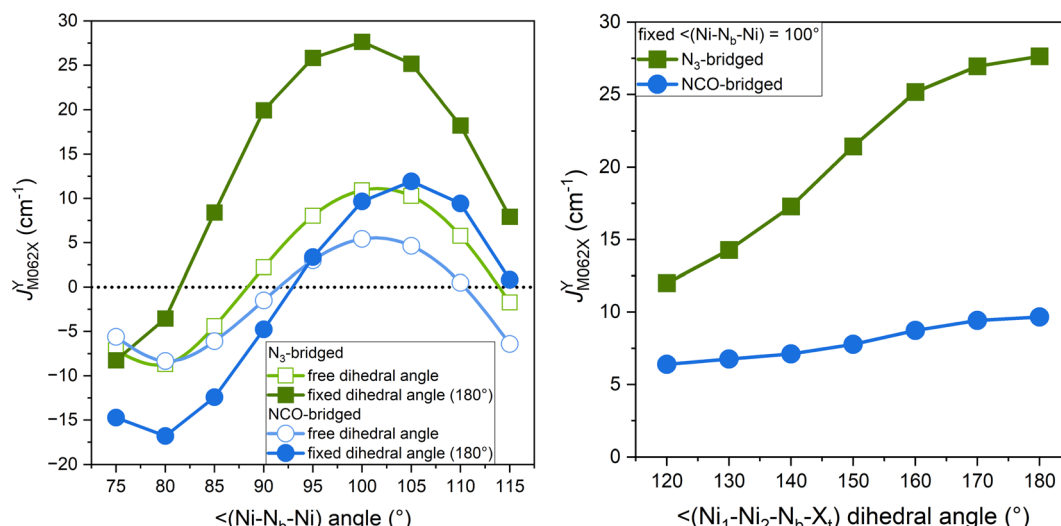


Fig. 8 Magneto-structural correlation for model complexes $[\text{Ni}_2(\mu_{1,1}-\text{N}_3)_2(\text{NH}_3)_8]^{2+}$ and $[\text{Ni}_2(\mu_{1,1}-\text{NCO})_2(\text{NH}_3)_8]^{2+}$ calculated with M06-2X functional.

Conclusion

We have synthesized and structurally characterized two new doubly $\mu_{1,1}\text{-N}_3$ bridged and six new doubly $\mu_{1,1}\text{-NCO}$ bridged Ni^{II} complexes with the six different N_3O donor Schiff base ligands. All these neutral complex molecules are isostructural and construct edge sharing bioctahedral structures. Magnetic studies revealed that all these complexes exhibit ferromagnetic interaction through bridging pseudohalides with ferromagnetic coupling constant J being significantly higher for azide-bridged complexes than that of the cyanate analogues, which is consistent with the literature reported data and also the presence of polarizable π systems and two different N and O donor atoms in cyanate ion, rendering it to be a poor magnetic coupler in comparison to azide analogues. Although, the magneto-structurally characterized doubly $\mu_{1,1}\text{-N}_3$ bridged Ni^{II} complexes are abundant, only few such complexes with doubly $\mu_{1,1}\text{-NCO}$ bridged systems are known in the literature. Interestingly, inclusion of these six new examples in this ever-growing series of doubly $\mu_{1,1}\text{-NCO}$ bridged systems gives us an opportunity to analyse the precise magneto-structural correlation in this system, showing a general trend in which J value increases with increase in bridging angles, similar to theoretical prediction that has been conducted by Ruiz *et al.* for azide analogues. Therefore, the unprecedented high degree of structural and magnetic resemblances by inclusion of six new examples in this series is the major achievement of the present study. Moreover, very detailed DFT study fully confirmed that N_3 -ligand is prominent to NCO-ligand in promoting ferromagnetic exchange and that accurate magneto-structural correlation of such Ni^{II} dinuclear complexes is two-dimensional, based on $\text{Ni-N}_b\text{-Ni}$ bond angles and $\text{Ni}_1\text{-Ni}_2\text{-N}_b\text{-X}_t$ dihedral angles.

Conflicts of interest

There are no conflicts to declare.

Acknowledgements

A. P. gratefully acknowledges the financial support of this work by the Government of West Bengal through the Department of Science & Technology and Biotechnology, Kolkata, India (Sanction No. 331/ST/P/S&T/15G-8/2018, dated-19.06.2019). P. B. gratefully acknowledges the financial support of this work by the project CICECO-Aveiro Institute of Materials, UIDB/50011/2020, UIDP/50011/2020 & LA/P/0006/2020, financed by national funds through the FCT/MCTES (PIDAAC). R. H. acknowledges the financial support from the institutional sources of the Department of Inorganic Chemistry, Palacký University Olomouc, Czech Republic.

References

- 1 G. A. Craig and M. Murrie, *Chem. Soc. Rev.*, 2015, **44**, 2135–2147.
- 2 G. E. Kostakis, A. M. Ako and A. K. Powell, *Chem. Soc. Rev.*, 2010, **39**, 2238–2271.
- 3 M. Andruh, *Chem. Commun.*, 2018, **54**, 3559–3577.
- 4 M. Mondal, S. Ghosh, S. Maity, S. Giri and A. Ghosh, *Inorg. Chem. Front.*, 2020, **7**, 247–259.
- 5 X.-Y. Wang, Z.-M. Wang and S. Gao, *Chem. Commun.*, 2008, 281–294.
- 6 M. Sarkar, R. Clérac, C. Mathonière, N. G. R. Hearns, V. Bertolasi and D. Ray, *Inorg. Chem.*, 2011, **50**, 3922–3933.
- 7 K. Aoki, K. Otsubo, Y. Yoshida, Y. Kimura, K. Sugimoto and H. Kitagawa, *Inorg. Chem.*, 2021, **60**, 16029–16034.
- 8 N. C. Jana, Z. Jagličić, P. Brandão, S. Adak, A. Saha and A. Panja, *New J. Chem.*, 2021, **45**, 7602–7613.
- 9 S. Khan, T. Dutta, M. Cortijo, R. González-Prieto, M. G. B. Drew, R. M. Gomila, A. Frontera and S. Chattopadhyay, *CrystEngComm*, 2021, **23**, 1942–1952.
- 10 (a) S. Sasmal, S. Hazra, P. Kundu, S. Dutta, G. Rajaraman, E. C. Sañudo and S. Mohanta, *Inorg. Chem.*, 2011, **50**,





7257–7267; (b) P. Bhunia, S. Maity, J. Mayans and A. Ghosh, *New J. Chem.*, 2022, **46**, 4363–4372; (c) H. S. Jena, S. Goswami, S. Sanda, S. Parshamoni, S. Biswas and S. Konar, *Dalton Trans.*, 2014, **43**, 16996–16999.

11 A. Escuer, J. Esteban, S. P. Perlepes and T. C. Stamatatos, *Coord. Chem. Rev.*, 2014, **275**, 87–129.

12 L. Botana, J. Ruiz, A. J. Mota, A. Rodríguez-Diéguez, J. M. Seco, I. Oyarzabal and E. Colacio, *Dalton Trans.*, 2014, **43**, 13509–13524.

13 R. Boča, *Coord. Chem. Rev.*, 2004, **248**, 757–815.

14 J. Miklovič, D. Valigura, R. Boča and J. Titiš, *Dalton Trans.*, 2015, **44**, 12484–12487.

15 R. Maurice, *Inorg. Chem.*, 2021, **60**, 6306–6318.

16 B. Drahoš and R. Herchel, *Dalton Trans.*, 2022, **51**, 18033–18044.

17 A. Escuer, R. Vicente, M. S. E. Fallah, X. Solans and M. Font-Bardia, *J. Chem. Soc., Dalton Trans.*, 1996, 1013.

18 Z. Mahendrasinh, S. Ankita, S. B. Kumar, A. Escuer and E. Suresh, *Inorg. Chim. Acta*, 2011, **375**, 333–337.

19 M. Habib, T. K. Karmakar, G. Aromí, J. Ribas-Ariño, H.-K. Fun, S. Chantrapromma and S. K. Chandra, *Inorg. Chem.*, 2008, **47**, 4109–4117.

20 M. I. Arriortua, R. Cortes, J. L. Mesa, L. Lezama, T. Rojo and G. Villeneuve, *Transition Met. Chem.*, 1988, **13**, 371–374.

21 A. Panja, N. C. Jana, S. Adak, P. Brandão, L. Dlháň, J. Titiš and R. Boča, *New J. Chem.*, 2017, **41**, 3143–3153.

22 M. Patra, P. Brandão, A. P. Pikul, S. Adak and A. Panja, *ChemistrySelect*, 2020, **5**, 12924–12931.

23 S. Adak, Y.-C. Sun, N. C. Jana, P. Brandão, X.-Y. Wang and A. Panja, *CrystEngComm*, 2021, **23**, 3371–3382.

24 E. Ruiz, J. Cano, S. Alvarez and P. Alemany, *J. Am. Chem. Soc.*, 1998, **120**, 11122–11129.

25 F. F. de Biani, E. Ruiz, J. Cano, J. J. Novoa and S. Alvarez, *Inorg. Chem.*, 2000, **39**, 3221–3229.

26 (a) P. S. Perlepe, L. Cunha-Silva, K. J. Gagnon, S. J. Teat, C. Lampropoulos, A. Escuer and T. C. Stamatatos, *Inorg. Chem.*, 2016, **55**, 1270–1277; (b) M. K. Mahish, L. M. Carrella, A. Patra, D. Saren, E. Zangrandino, P. Vojtěšek, E. Rentschler and S. C. Manna, *New J. Chem.*, 2022, **46**, 16899–16906; (c) A. Panja, S. Adak, P. Brandão, L. Dlháň and R. Boča, *Eur. J. Inorg. Chem.*, 2020, 2362–2371.

27 A. Panja, Z. Jagličić, R. Herchel, P. Brandão, K. Pramanik and N. C. Jana, *New J. Chem.*, 2022, **46**, 5627–5637.

28 A. Panja, Z. Jagličić, R. Herchel, P. Brandão, K. Pramanik and N. C. Jana, *New J. Chem.*, 2022, **46**, 13546–13557.

29 G. M. Sheldrick, SADABS, University of Göttingen, Germany, 1996.

30 G. M. Sheldrick, *Acta Crystallogr., Sect. A: Found. Crystallogr.*, 2008, **64**, 112.

31 S. S. Massoud, F. R. Louka, Y. K. Obaid, R. Vicente, J. Ribas, R. C. Fischer and F. A. Mautner, *Dalton Trans.*, 2013, **42**, 3968–3978.

32 M. G. Barandika, R. Cortés, L. Lezama, M. K. Urtiaga, M. I. Arriortua and T. Rojo, *J. Chem. Soc., Dalton Trans.*, 1999, 2971–2976.

33 P. Mukherjee, M. G. B. Drew, C. J. Gómez-García and A. Ghosh, *Inorg. Chem.*, 2009, **48**, 5848–5860.

34 S. K. Dey, N. Mondal, M. S. E. Fallah, R. Vicente, A. Escuer, X. Solans, M. Font-Bardia, T. Matsushita, V. Gramlich and S. Mitra, *Inorg. Chem.*, 2004, **43**, 2427–2434.

35 S. Sarkar, A. Mondal, M. S. E. Fallah, J. Ribas, D. Chopra, H. Stoeckli-Evans and K. K. Rajak, *Polyhedron*, 2006, **25**, 25–30.

36 S. Nandi, D. Bannerjee, J.-S. Wu, T.-H. Lu, A. M. Z. Slawin, J. D. Woollins, J. Ribas and C. Sinha, *Eur. J. Inorg. Chem.*, 2009, 3972–3981.

37 P. Chaudhuri, R. Wagner, S. Khanra and T. Weyhermüller, *Dalton Trans.*, 2006, 4962–4968.

38 A. Bhattacharyya, P. K. Bhaumik, M. Das, A. Bauzá, P. P. Jana, K. Harms, A. Frontera and S. Chattopadhyay, *Polyhedron*, 2015, **101**, 257–269.

39 M. Č. Romanović, B. R. Čobeljić, A. Pevec, I. Turel, V. Spasojević, A. A. Tsaturyan, I. N. Shcherbakov, K. K. Andelković, M. Milenković, D. Radanović and M. R. Milenković, *Polyhedron*, 2017, **128**, 30–37.

40 P. Ghorai, P. Brandão, S. Benmansour, C. J. Gómez García and A. Saha, *Polyhedron*, 2020, **188**, 114708.

41 P. P. Chakrabarty, S. Giri, D. Schollmeyer, H. Sakiyama, M. Mikuriya, A. Sarkar and S. Saha, *Polyhedron*, 2015, **89**, 49–54.

42 H.-Z. Kou, S. Hishiya and O. Sato, *Inorg. Chim. Acta*, 2008, **361**, 2396–2406.

43 S. Sarkar, A. Mondal, A. Banerjee, D. Chopra, J. Ribas and K. K. Rajak, *Polyhedron*, 2006, **25**, 2284–2288.

44 S. Sarkar, A. Datta, A. Mondal, D. Chopra, J. Ribas, K. K. Rajak, S. M. Sairam and S. K. Pati, *J. Phys. Chem. B*, 2006, **110**, 12–15.

45 X.-J. Lin, Z. Shen, Y. Song, H.-J. Xu, Y.-Z. Li and X.-Z. You, *Inorg. Chim. Acta*, 2005, **358**, 1963–1969.

46 S. Sain, S. Bid, A. Usman, H.-K. Fun, G. Aromí, X. Solans and S. K. Chandra, *Inorg. Chim. Acta*, 2005, **358**, 3362–3368.

47 R. Cortes, J. I. Ruiz de Larramendi, L. Lezama, T. Rojo, K. Urtiaga and M. I. Arriortua, *J. Chem. Soc., Dalton Trans.*, 1992, 2723–2728.

48 R. Vicente, A. Escuer, J. Ribas, M. S. E. Fallah, X. Solans and M. Font-Bardia, *Inorg. Chem.*, 1993, **32**, 1920–1924.

49 J. Ribas, M. Monfort, C. Diaz, C. Bastos and X. Solans, *Inorg. Chem.*, 1994, **33**, 484–489.

50 A. Escuer, R. Vicente, J. Ribas and X. Solans, *Inorg. Chem.*, 1995, **34**, 1793–1798.

51 A. Donmez, G. Oylumluoglu, M. B. Coban, C. Kocak, M. Aygun and H. Kara, *J. Mol. Struct.*, 2017, **1149**, 569–575.

52 N. F. Chilton, R. P. Anderson, L. D. Turner, A. Soncini and K. S. Murray, *J. Comput. Chem.*, 2013, **34**, 1164–1175.

53 G. Manca, J. Cano and E. Ruiz, *Inorg. Chem.*, 2009, **48**, 3139–3144.

54 H.-D. Bian, W. Gu, Q. Yu, S.-P. Yan, D.-Z. Liao, Z.-H. Jiang and P. Cheng, *Polyhedron*, 2005, **24**, 2002–2008.

55 F. Neese, *Wiley Interdiscip. Rev.: Comput. Mol. Sci.*, 2022, **12**, e1606.

56 E. Ruiz, J. Cano, S. Alvarez and P. Alemany, *J. Comput. Chem.*, 1999, **20**, 1391–1400.

57 T. Soda, Y. Kitagawa, T. Onishi, Y. Takano, Y. Shigeta, H. Nagao, Y. Yoshioka and K. Yamaguchi, *Chem. Phys. Lett.*, 2000, **319**, 223–230.

58 (a) A. D. Becke, *Phys. Rev. A*, 1988, **38**, 3098–3100; (b) C. Lee, W. Yang and R. G. Parr, *Phys. Rev. B: Condens. Matter Mater. Phys.*, 1988, **37**, 785–789; (c) P. J. Stephens, F. J. Devlin, C. F. Chabalowski and M. J. Frisch, *J. Phys. Chem.*, 2002, **98**, 11623–11627.

59 Y. Zhao and D. G. Truhlar, *Theor. Chem. Acc.*, 2008, **120**, 215–241.

60 (a) L. Havlíček, R. Herchel, I. Nemec and P. Neugebauer, *Polyhedron*, 2022, **223**, 115962; (b) A. Bhanja, L. Smythe, R. Herchel, I. Nemec, M. Murrie and D. Ray, *Dalton Trans.*, 2021, **50**, 5023–5035; (c) B. Rybníčková, J. Kuchár, P. Antal and R. Herchel, *Inorganica Chim. Acta*, 2020, **509**, 119689; (d) R. Herchel, I. Nemec, M. Machata and Z. Trávníček, *Inorg. Chem.*, 2015, **54**, 8625–8638.

61 M. Zlatar, F. Vlahović, D. Mitić, M. Zlatović and M. Gruden, *J. Serbian Chem. Soc.*, 2020, **85**, 1577–1590.

62 C. van Wüllen, *J. Chem. Phys.*, 1998, **109**, 392–399.

63 F. Weigend and R. Ahlrichs, *Phys. Chem. Chem. Phys.*, 2005, **7**, 3297–3305.

64 C. F. Macrae, I. Sovago, S. J. Cottrell, P. T. A. Galek, P. McCabe, E. Pidcock, M. Platings, G. P. Shields, J. S. Stevens, M. Towler and P. A. Wood, *J. Appl. Crystallogr.*, 2020, **53**, 226–235.

65 C. R. Groom, I. J. Bruno, M. P. Lightfoot and S. C. Ward, *Acta Crystallogr. B. Struct.*, 2016, **72**, 171–179.

